

1 **Modified protein expression in the tectorial membrane of the cochlea reveals roles for**
2 **the striated sheet matrix**

3 G. P. Jones,^{†1} S. J. Elliott,[‡] I. J. Russell,^{†*} and A. N. Lukashkin^{†*}

4 [†]School of Pharmacy and Biomolecular Sciences, University of Brighton, Brighton, BN2
5 4GJ, UK

6 [‡]Institute of Sound and Vibration Research, University of Southampton, Southampton, SO17
7 1BJ, UK

8 ¹Present address: University College London Ear Institute, 332 Grays Inn Road, London,
9 WC1X 8EE, UK

10 *Correspondens: A.Lukashkin@brighton.ac.uk or I.Russell@brighton.ac.uk

11 Short title: Roles for the striated sheet matrix

12 Keywords: cochlear amplifier, cochlear model, cochlear sensory processing, organ of Corti,
13 genetically related deafness

14

15

16

17

18

19

20

21

22 **ABSTRACT**

23 The tectorial membrane (TM) of the mammalian cochlea is a complex extracellular matrix
24 which, in response to acoustic stimulation, displaces the hair bundles of outer hair cells
25 (OHCs), thereby initiating sensory transduction and amplification. Here, using TM segments
26 from the basal, high-frequency, region of the cochleae of genetically modified mice
27 (including models of human hereditary deafness) with missing or modified TM proteins, we
28 demonstrate that frequency-dependent stiffening is associated with the striated sheet matrix
29 (SSM). Frequency-dependent stiffening largely disappeared in all three TM mutations studied
30 where the SSM was absent either entirely or at least from the stiffest part of the TM overlying
31 the OHCs. In all three TM mutations, dissipation of energy is decreased at low (< 8 kHz) and
32 increased at high (> 8 kHz) stimulus frequencies. The SSM is composed of polypeptides
33 carrying fixed charges and electrostatic interaction between them may account for frequency-
34 dependent stiffness changes in the material properties of the TM. Through comparison with
35 previous *in vivo* measurements, it is proposed that implementation of frequency-dependent
36 stiffening of the TM in the OHC attachment region, facilitates interaction between tones,
37 backward transmission of energy, and amplification in the cochlea.

38

39

40 INTRODUCTION

41 The detection of sound in the mammalian cochlea is mediated via the organ of Corti (OC); a
42 remarkable integration of extracellular matrices, cytoskeletal architecture, and molecular
43 machinery. Each element of the OC has specific electrical and mechanical properties to
44 facilitate transmission of acoustic energy along the cochlea, decompose complex sounds into
45 individual frequency components, and, through rapid mechano-electrical – electromechanical
46 processes, amplify mechanical movements and convert them into electrical signals across
47 vast ranges of frequencies and levels (1). The stiffness of the basilar membrane (BM) of the
48 OC increases from the apex of the cochlea to its base (2). This gradient of stiffness provides
49 the mechanical basis for cochlear frequency tuning with low frequency vibrations of the BM
50 peaking near the apex of the cochlea and high frequencies peaking near the base (2).
51 Miniscule amounts of energy transmitted by the BM vibrations cause shear displacements
52 between the apical surface of the OC and another extracellular matrix, the tectorial
53 membrane (TM), into which the tips of the stereocilia of the outer hair cells (OHCs) are
54 imbedded (3). The resultant modulation of current flow through the OHC serves as a control
55 signal for the cochlear amplifier (4,5), which amplifies and sharpens the BM vibrations at the
56 frequency-specific place (6).

57 The TM is a viscoelastic structure (7) that decreases in both width and thickness from cochlea
58 apex to base and has longitudinal anisotropy (8-12) that parallels that of the BM (6).
59 Interaction between BM and TM travelling waves has been hypothesised to control the
60 spatial extent and timing of OHC excitation, which affects both gain and frequency tuning in
61 the cochlea (13-16). Timing of the TM and BM travelling waves determines the relative shear
62 motion between the OC and the TM (17,18). Recently, it was found that the mechanical
63 properties of the TM varied with stimulus frequency (19); a property that has yet to be
64 considered in cochlear models. According to this new finding, energy transmission along the
65 various structures in the cochlea, which are submerged in fluid, is optimised, thereby
66 enhancing amplification of signals at the frequency-specific place, (19). The
67 structural/physicochemical basis for the frequency dependence of the TM's mechanical
68 properties is, however, unknown.

69 The structural complexity of the mammalian TM (20) has been associated with recent
70 findings that reveal important roles for the TM in the harnessing and distribution of energy
71 and frequency tuning in the mammalian cochlea (14,15,21-23). Despite advances in

72 understanding the physiological importance of the TM, it is not known, as yet, which part of
73 the TM's intricate structure is responsible for its complex, frequency-dependent material
74 properties. The most complex structural component of the TM appears to be the core, which
75 is composed of radial bands of collagen fibres imbedded in and structurally organised by a
76 striated sheet matrix (SSM); a quasi-crystalline array of glycoproteins (24,25). The SSM is
77 composed of a number of different proteins, including α -tectorin (Tecta) (21,26,27), β -
78 tectorin (Tectb) (14,22), otogelin (28), otolin (29), and Ceacam16 (30), which have been
79 ascribed with organising the longitudinal anisotropy of the TM (9-12,31). In this paper we
80 describe the outcome of experiments designed to determine the frequency-dependent material
81 properties of TM segments extracted from three groups of mice with disrupted or missing
82 SSM. The groups with missing SSM comprise *Tecta*^{Y1870C/+}, lacking expression of α -tectorin
83 (21) and *Tectb*^{-/-}, lacking expression of β -tectorin (14). In the third group, *Otoa*^{EGFP/EGFP}
84 mice, which lack the expression of otoancorin (23,32), although the structure of SSM is
85 largely unaffected, the SSM is missing from the region overlying the OHCs (23). In humans,
86 mutations of *Tecta*^{Y1870C/+} and *Otoa*^{EGFP/EGFP} are causes of hereditary deafness (10,33,34). We
87 used a laser interferometer to measure the longitudinal propagation of radial, shearing,
88 travelling-waves along the lengths of TM segments isolated from the basal, high-frequency,
89 turns of the cochleae. The outcomes of these measurements are discussed with respect to
90 known physicochemical properties of the TM and *in vivo* measurements of the acoustical,
91 mechanical and electrical responses of the cochlea.

92 MATERIALS AND METHODS

93 Preparation of TM samples

94 Data from the basal cochlear region were collected from *Tecta*^{Y1870C/+}, *Tectb*^{-/-}, and
95 *Otoa*^{EGFP/EGFP} mice on CBA/Ca backgrounds, between 1 and 6 months of age. Mice were
96 euthanised by CO₂ and dissections were performed under a light microscope, in a Petri dish
97 containing artificial endolymph (174 mMol KCl, 2.00 mMol NaCl, 0.0261 mMol CaCl₂,
98 3.00 mMol D-glucose, 5.00 mMol HEPES, pH=7.3). The inner ear was removed from the
99 skull and the cochlea was opened with forceps. The TM was detached from the spiral limbus
100 (if necessary) using a tungsten probe with a tip diameter of <0.1 mm, and cut with a scalpel
101 blade into segments between 350-1000 μ m long. A segment cut from the basal 3rd of the
102 detached TM, was transferred into the pre-prepared experimental chamber using a glass
103 tipped pipette and mounted.

104 **Travelling wave excitation and measurements**

105 Experiments were conducted using the method previously described (19) in a quiet room, on
 106 a vibration isolation table, and inside a Faraday cage. The experimental chamber was filled
 107 with artificial endolymph so that the prepared TM was submerged to a depth of at least 4 mm.
 108 Cell-Tak (BD Biosciences) was used to attach a single segment of TM to a vibrating support
 109 ($\sim 5 \times 10 \times < 1$ mm) attached to a stimulation piezo (Thorlabs AE0203D04), and a mechanically
 110 isolated stationary support ($\sim 10 \times 10 \times < 1$ mm) (Fig. 1). The stimulation piezo was mounted
 111 rigidly to the microscope slide forming the base of the chamber. A lab built, self-mixing,
 112 homodyne laser-diode interferometer (35) aimed through a viewing window in the front wall
 113 and was used to record the phase and amplitude of travelling wave at multiple points along
 114 the mounted segment of TM. The beam of the laser interferometer was focused onto the
 115 marginal edge of the TM near the vibrating support so that the light entering the chamber was
 116 approximately parallel with the end of the vibrating support. Recording commenced from this
 117 point and the laser beam was stepped along the TM (in 10 or 20 μm steps, typically with 3-5
 118 repetitive measurements for each position) until it came within 100 μm of the stationary
 119 support or a segment of at least 300 μm had been covered for each TM preparation. Radial
 120 sinusoidal stimulation of 2-20 kHz was applied to the TM via the vibrating support in steps of
 121 1 kHz at every longitudinal position. Measurements below 2 kHz and above 20 kHz were not
 122 reliable due to small phase gradients at lower frequencies and small amplitude of vibrations
 123 and, hence, low signal-to-noise ratio at high frequencies. Amplitude data were calibrated to
 124 control for variable reflectance at each point along the TM using a piezo with known
 125 displacement, on which the laser diode was mounted.

126 **Calculation of material properties of the TM**

127 Shear modulus, $G'(\omega)$, and shear viscosity, $\eta(\omega)$ of the TM were calculated using a model
 128 of the TM in fluid environment (19). Namely, shear modulus and shear viscosity were
 129 calculated from the equation

$$G'(\omega) + i\omega\eta(\omega) = \frac{\omega^2\rho_f(T_{TM} + \sqrt{2}\delta) - i\sqrt{2}\omega^2\rho_f\delta}{k^2(\omega)T_{TM}}, \quad (1)$$

130 where ω is angular frequency, T_{TM} is thickness of the TM (2×10^{-5} m), ρ_f is the fluid density
 131 (10^3 kg m^{-3}), k is the complex wavenumber and δ is the boundary layer thickness, which was
 132 determined as

$$\delta = \sqrt{\frac{\mu}{\omega \rho_f}}, \quad (2)$$

133 where μ is the coefficient of viscosity ($7 \times 10^{-4} \text{ kg m}^{-1} \text{ s}^{-1}$). The complex wavenumber can be
 134 calculated from the measured wave speed, c , and decay constant, α , as

$$k = \frac{\omega}{c} - i\alpha. \quad (3)$$

135 RESULTS

136 Frequency dependent propagation of longitudinal travelling waves was investigated in
 137 segments of TM isolated from the basal (high-frequency) region of cochleae from
 138 *Tecta*^{Y1870C/+}, *Tectb*^{-/-} and *Otoa*^{EGFP/EGFP} mice, with mutations or deletions of the TM proteins,
 139 α -tectorin, β -tectorin, and otoancorin. Measurements were confined to the basal region,
 140 because it was in this region that the propagation of longitudinal travelling waves along the
 141 TM showed greatest frequency dependency (19). Longitudinally propagating travelling shear
 142 waves were excited in the TM by sinusoidal vibration of the piezoelectric actuator (Fig. 1)
 143 and the magnitude and phase of the radial displacement due to the travelling wave, as
 144 functions of distance from the source of excitation, were measured with a laser diode
 145 interferometer (35). These data provided the basis for deriving the dynamic material
 146 properties of the TM.

147 **Velocity of the TM travelling waves decreases when SSM is disrupted or missing**

148 The travelling wave velocity was calculated from the progressive phase lag measured as a
 149 function of longitudinal distance from the vibrating platform ($x=0 \text{ } \mu\text{m}$). In modified TMs
 150 from all three groups of mice, the phase lag increased as a function of stimulation frequency
 151 (2-20 kHz) (Fig. 2 A-C).

152 The propagation velocity, c , of the travelling waves was calculated at each frequency, ω , as
 153 $c = \omega \times x / \Delta\phi$, where $\Delta\phi$ is the overall change in phase over the longest measurement
 154 distance x for each segment, i.e. average velocity over distance x was calculated. The means
 155 and standard error of c at each frequency are shown in Fig. 2 D and compared to previously
 156 published data from normal, wild-type TMs (19).

157 Propagation velocity in TM segments taken from mice with disrupted or missing SSM
 158 increased as a function of stimulus frequency. The velocity increase with frequency was

159 similar for all three groups, increasing from $\sim 1.5 \text{ m s}^{-1}$ at 2 kHz to 5.5 m s^{-1} at 20 kHz. Apart
 160 from the propagation velocity minima at 5 kHz, propagation velocities measured from the
 161 wild-type mice (black squares, Fig. 2 D) are significantly higher than those measured in the
 162 groups with modified TM, especially at the highest stimulus frequency used (20 kHz).

163 **Amplitude decay of TM travelling wave increases when SSM is disrupted or missing**

164 The amplitude of the travelling wave also decays with distance along the TM. The decay
 165 constant, α , was derived by fitting an exponential decay to the wave amplitude, $Y(x)$ as a
 166 function of longitudinal distance x , namely, $Y(x) = Y(0)e^{-\alpha x}$, where $Y(0)$ is the wave
 167 amplitude at the stimulation place.

168 The decay constant tended to decrease with increasing stimulus frequency in TM segments
 169 isolated from the wild-type mice ((19), squares in Fig. 3). For all three groups with modified
 170 SSM, however, the decay constant increased with increasing frequency over the same
 171 stimulus frequency range (Fig. 3). An increase in α corresponds to a decrease in the space
 172 constant (σ), which represents the spatial extent of the wave's propagation (Fig. 3).

173 **The mechanical properties of the TM are affected by structural disruption of SSM**

174 The viscoelastic properties, namely the shear storage modulus, $G'(\omega)$, and shear viscosity,
 175 $\eta(\omega)$, were calculated at discrete frequencies from the wave propagation velocity, $c(\omega)$, and
 176 the decay constant, $\alpha(\omega)$, using Eqs. 1 and 3 (Materials and Methods). These properties had
 177 previously been found to be highly dependent on stimulus frequency when measured from
 178 TM segments isolated from the basal turn of the wild-type mice (19). The shear viscosity,
 179 $\eta(\omega)$, which was shown in the wild-type mice to decrease markedly with increasing
 180 frequency (squares, Fig. 4 B), was found here to be independent of frequency in all three
 181 groups with disrupted or missing SSM (circles, crosses and triangles, Fig. 4 B). The shear
 182 storage modulus, $G'(\omega)$, measured from TM segments isolated from the basal region of all
 183 three groups of mice with modified TMs increased as a function of stimulus frequency, from
 184 2.52 to 31.2 kPa for *Tecta*^{Y1870C/+}, 4.46 to 29.7 kPa for *Tectb*^{-/-}, and 4.63 to 41.2 kPa for
 185 *Otod*^{EGFP/EGFP}, between 2-20 kHz (circles, crosses and triangles, Fig. 4 A). These increases
 186 are small when compared with those obtained from similar measurements made from wild-
 187 type mice, where $G'(\omega)$ increased over the same stimulus frequency range from 6.50 kPa to
 188 80.1 kPa (squares, Fig. 4 A).

189 **Energy transmission and dissipation is modified in TMs with disrupted SSM**

190 The loss tangent $\tan(\delta) = G''/G'$, where G'' is the loss modulus (G'' is calculated as $G'' =$
 191 $\omega\eta(\omega)$ using data for $\eta(\omega)$ in Fig. 4 B), defines the ratio of energy dissipated to energy
 192 stored per volume unit of TM (19) and characterises the effectiveness of longitudinal energy
 193 transmission during shear deformations of the TM (Fig. 4 C). $\tan(\delta)$ calculated for the TM
 194 segments isolated from the basal regions of the three groups with modified TM (circles,
 195 crosses and triangles, Fig. 4 C) behaved differently as functions of stimulus frequency to that
 196 of basal turn TM segments of wild-type mice (squares, Fig. 4 C). For stimulus frequencies
 197 below 5 kHz, $\tan(\delta)$ calculated for TM segments isolated from the groups with disrupted or
 198 missing SSM was significantly lower than that of $\tan(\delta)$ calculated for TM segments of the
 199 wild-type mice. In other words, at these low frequencies, the relative dissipation of energy is
 200 lower in the modified TMs than in the wild-type mice. At 20 kHz, however, $\tan(\delta)$ for the
 201 wild-type mice is about half of that for any group with disrupted or missing SSM and, hence,
 202 the TM in the wild-type mice is more efficient at transmitting energy at stimulus frequencies
 203 approaching the frequency range of the basal turn of the mouse cochlea.

204 The reciprocal of the loss tangent is proportional to the quality factor, ($Q \propto 1/\tan(\delta) =$
 205 G'/G''), which describes the resonant material properties of the TM (Fig. 4 D). In the
 206 segments from all groups with modified TMs (circles, crosses and triangles, Fig. 4 D), Q is
 207 relatively independent of frequency, while in the TM segments isolated from the wild-type
 208 mice (squares, Fig. 4 D), there is a very clear rise in the value of Q with increasing frequency.
 209 In all three groups with disrupted or missing SSM there is less variation in Q with frequency
 210 across the 2-20 kHz range, than in segments isolated from the wild-type cochleae.

211 **DISCUSSION**

212 ***In vitro* travelling wave propagation is disrupted in all three mutant groups with** 213 **compromised striated sheet matrix**

214 The velocities of travelling waves measured in segments of TM isolated from the cochleae of
 215 *Tecta*^{Y1870C/+}, *Tectb*^{-/-} and *Otoa*^{EGFP/EGFP} mice were all similarly and significantly reduced by
 216 comparison with travelling wave velocities measured in segments of TM isolated from the
 217 same region of the cochleae of wild-type mice (Fig. 2 D). Reductions in the wave velocity
 218 were accompanied by an increase in the decay constant for the majority of the measured
 219 frequency range (Fig. 3) and are manifested in travelling waves (Fig. 5), which have shorter
 220 wavelengths with more rapid decay than those from wild-type TMs. We attribute these

221 differences largely to changes in frequency dependant stiffness than to shear viscosity. This is
222 because, at least for the frequencies illustrated in Fig. 5 (> 8 kHz), the shear viscosity of TMs
223 isolated from wild-type mice and those with genetically modified protein composition are
224 similar (Fig. 4 B). The only major structural component of the TM, which, as far as we are
225 aware, is altered in common in the genetically modified mice used in this study, is the SSM.
226 It is completely absent in the *Tectb*^{-/-} mouse (14) and partially lost in the *Tecta*^{Y1870C/+} mouse
227 (21), including a marginal region where, in the TM of *Otod*^{EGFP/EGFP} mice, it is specifically
228 absent. The marginal region is a zone 20 µm wide (~20% width of the TM), which runs along
229 the lateral edge that overlies the OHCs (23). It is the stiffest part of the TM and, in the basal
230 turn of the cochlea, is the only region of the TM that becomes increasingly stiffer with
231 increasing frequency place on the BM (8,36). Gueta et al. (36) presumed that the place-
232 dependent stiffness gradient of this zone was to facilitate energy transfer with the OHC hair
233 bundles, whose stiffness also increases with increasing distance from the apex of the cochlea
234 (37,38). It would appear, according to the findings reported here, that any loss of SSM,
235 especially in the hair bundle attachment zone of the TM, is associated with a loss of the
236 frequency-dependent stiffness of the material properties of the TM.

237 Findings related to the frequency-dependency of mechanical properties of the TM reported
238 here are new and novel, although the measurements of the mechanical properties of the TM
239 upon which they are based are similar to those reported previously for individual frequencies,
240 using similar methods, from mice with genetic modification of the TM (22,39).

241 **Disruption or absence of the striated sheet matrix largely abolishes frequency**
242 **dependence of the TM mechanical properties**

243 The organization of the TM is complex with radial collagen fibres and interconnecting non-
244 collagenous glycoproteins forming the quasi-crystalline striated sheet matrix (24,25). This
245 complexity has led to the suggestion that the array structure and different packing density of
246 collagen fibres form a basis for longitudinal, radial and transversal gradients of the TM's
247 mechanical properties (8-12). We would like to suggest further that the striated sheet matrix
248 provides a specific structural basis for the frequency dependency of the material properties of
249 the TM (19).

250 Insight into the physical basis for the frequency dependence of the mechanical properties of
251 the TM may be deduced from what is currently understood about the physical chemistry of
252 the TM. In a recent conceptual model, the TM is considered as a porous matrix, consisting of

253 solid and fluid phases with the fluid phase moving through pores of a limited size (40). At
254 asymptotically low frequencies, the elasticity of the solid phase, namely the elasticity of
255 interconnected collagen fibres, is the dominating component of the TM stiffness. With
256 increasing stimulation frequency the viscosity of fluid moving through the relatively small
257 pores of the TM matrix would be expected to contribute significantly towards the TM's
258 mechanical properties, thereby creating a possible basis for their frequency dependence.
259 Indeed, changes in the viscosity of the TM's fluid phase are associated with prominent
260 changes in TM electrokinetic response (41), indicating the importance of fluid movement
261 within the TM during its deformation. If in TMs with missing or genetically modified
262 proteins, the porous structure is altered, as found by Masaki et al. (39) for TM isolated from
263 *Tecta*^{Y1870C/+} mice, the contribution from the viscosity of the fluid phase might be reduced
264 with a consequent reduction or abolition of the frequency dependency of the TM mechanical
265 properties. Such changes in the shear viscosity of the TM has been shown to modify
266 propagation of waves in the TM with important consequences for cochlear tuning in
267 *Tecta*^{Y1870C/+} mice (42).

268

269 Another possible basis for the frequency dependent mechanical properties of the TM is
270 changes in the local density of fixed charges within the TM during its deformation. It has
271 been demonstrated that the TM contains high concentration of fixed charges associated with
272 ionized sulfate (SO₃⁻) and carboxyl (COO⁻) groups of glycoproteins (7,43) and that
273 electrostatic interaction between them contributes significantly to the compressional stiffness
274 of the TM (41). Furthermore, neutralization of the fixed charges at low pH causes a two-
275 threefold reduction in the TM shear impedance (44). Thus shear deformation of the TM
276 should lead to changes in the local density of the fixed charges and consequent redistribution
277 of mobile ions and fluid phase within the TM according to the principles of electrodiffusive,
278 osmotic, and mechanical equilibrium, and bulk electroneutrality (43). The time taken to
279 reach the equilibrium is limited by the poroelastic relaxation time, which is of the order of
280 tens of minutes (7,40,45) and can affect the mechanical responses of the TM at acoustic
281 frequencies (41). If electrostatic interaction between the fixed charges contributes to the
282 frequency dependence of the TM mechanical properties then the decreased frequency
283 dependent stiffness we have observed in TMs from *Tecta*^{Y1870C/+}, *Tectb*^{-/-}, and *Otod*^{EGFP/EGFP}
284 mice could be due to a consequent reduction in density of the associated fixed charges in the
285 TM, as has indeed been reported for *Tecta*^{Y1870C/+} mice (39). A likely source of the fixed
286 charges, which is disrupted in all three mouse mutants used in this study, is the SSM which,

287 because of its composition and structural organisation, is likely to have a dense, highly
288 organised distribution of fixed charges.

289 Because both porosity and fixed charges within the TM determine its mechanical properties
290 (40,41,44) it is likely that combinations of both these factors determine specific frequency
291 dependence of the TM dynamic material properties (19). It should be remembered that
292 enhanced tuning of the TM (14) comes at a price. Fewer OHCs are engaged to amplify a
293 single frequency place on the BM, with subsequent loss, albeit relatively small, of sensitivity
294 (14,18). It would appear that sensitivity of the cochlea, rather than enhanced frequency tuning
295 of the TM has greater survival value.

296

297 **Forward energy transmission is not affected in mice with missing or disrupted striated** 298 **sheet matrix**

299 It has been hypothesised that a reduction of stiffness of the basal TM at low frequencies leads
300 to functional decoupling of the TM from the cochlear partition, which minimizes energy loss
301 and facilitates energy transmission along the cochlea to the cochlear apex (19). At the same
302 time, stiffening of the basal TM at high frequencies (19) maximizes cochlear amplifier gain
303 through better elastic coupling along the TM (14,16). The effectiveness of energy
304 transmission (loss tangent, $\tan(\delta)$, Fig. 4 C), which is relatively large at frequencies above 8
305 kHz for TM segments from mice with deleted or altered TM proteins compared to those of
306 TM segments from wild-type mice, is expected not to lead to higher energy losses from the
307 modified TMs *in vivo*. This is because the TM in the basal region of the cochlea would not
308 experience significant radial shear during the propagation of low-frequency BM travelling
309 waves. The waves peak at their characteristic frequency place, which is closer to the cochlear
310 apex, and do not show significant phase change in the basal region (6). *In vivo*, the TM in the
311 basal region of the cochlea experiences significant shear at frequencies that are close to the
312 CFs of that region (~35-60 kHz for the isolated TM segments used in our experiments).
313 Hence, higher energy losses from TMs of *Tecta*^{Y1870C/+}, *Tectb*^{-/-} and *Otoa*^{EGFP/EGFP} mice,
314 compared with wild-type mice, are expected only for frequencies near the characteristic
315 frequencies of the basal turn, but propagation of energy to the characteristic place should not
316 be affected.

317 **Physiological consequences of changes in mechanical properties of mutant TMs**
318 The physiological phenotypes expressed by *Tecta*^{Y1870C/+}, *Tectb*^{-/-}, and *Otoa*^{EGFP/EGFP} mice
319 reveal an important similarity and differences. Total loss of SSM, as in *Tectb*^{-/-} mice, is
320 associated with loss of elastic coupling along the TM *in vivo* (14,16) and, therefore the
321 presence of β -tectorin is necessary for maintaining the SSM and velocity and spatial extent of
322 travelling waves *in vitro* (15,19,22). In *Tectb*^{-/-} and *Tecta*^{Y1870C/+} mice, where SMM loss is not
323 restricted to the hair bundle attachment zone in the TM, gain and sensitivity of BM responses
324 in the 50-60 kHz region of the cochlea is reduced by ~10 dB SPL compared with
325 measurements from wild-type littermates (14,21) and *Otoa*^{EGFP/EGFP} mice (23). These
326 measurements, which reveal that the sensitivity of tone-evoked BM vibrations is changed
327 only slightly or imperceptibly, provide evidence that forward energy transmission is not
328 affected in the basal turn of the cochlea in these mutants. The loss of sensitivity of BM
329 motion measured in *Tectb*^{-/-} and *Tecta*^{Y1870C/+} mice, where there is total or partial loss of SSM
330 distributed throughout the TM, may be a consequence of imperfect impedance matching and
331 hence transfer of energy, between the stiffness of the OHC hair bundles and that of the TM;
332 or may be a consequence of changes in elastic (14,15,19) and viscous coupling (42) along the
333 TM with corresponding changes in the spread of excitation within the cochlea and reduction
334 in cochlear gain (14,16). *Tecta*^{Y1870C/+}, *Tectb*^{-/-}, and *Otoa*^{EGFP/EGFP} mice do, however, share a
335 common physiological phenotype. Changes in the mechanical properties of the TM of all
336 three mutants effect interaction between tones in the cochlea and the backward transmission
337 of energy from the cochlea, as a consequence of this interaction, as revealed in measurements
338 of DPOAE isothreshold responses. DPOAE thresholds are increased, in comparison with
339 those from wild-type littermates, by about 20 dB across the stimulus frequency range (2 – 60
340 kHz) in *Tecta*^{Y1870C/+} and *Otoa*^{EGFP/EGFP} mice (21,23). In addition, DPOAE generation in
341 *Tectb*^{-/-} mice appears to have a velocity dependency, possibly associated with loss of elastic
342 coupling along the TM. Thus for the products of interaction between tones in the cochlea, the
343 TM appears to act as the conduit for energy transfer along the organ of Corti, a process which
344 is severely attenuated in the TMs of mice where the SSM is missing, at least from the hair
345 bundle attachment zone of the TM. Regardless of what other structures have been implicated
346 in the transmission of emission energy along the cochlea (46), frequency-dependent
347 properties of the TM are essential for the generation and transmission of DPOAEs along the
348 BM. This finding has consequences in the clinic for subjects with congenital hearing loss due
349 to absence or modification of TM proteins, where there may be a mismatch between hearing
350 assessed through measurement of DPOAEs and more direct measures of cochlear responses.

351 **ACKNOWLEDGEMENTS**

352 We thank J. Hartley for the design and construction of electronic equipment and Guy
 353 Richardson for comments on an early version of the paper and for supplying the mice used in
 354 this study. This work is supported by a grant from the Medical Research Council. G.P.J. was
 355 supported by a BBSRC studentship.

356 **REFERENCES**

- 357 1. Russell, I. J. 2008. Cochlear receptor potentials. In *The Senses: A Comprehensive*
 358 *Reference*. A. I. Basbaum, A. Kaneko, G. M. Shepherd, G. Westheimer, T. D.
 359 Albright, R. H. Masland, P. Dallos, D. Oertel, S. Firestein, G. K. Beauchamp, M. C.
 360 Bushnell, J. H. Kaas, and E. Gardner, editors. Academic Press, New York. 319-358.
- 361 2. Békésy, G. v. 1960. *Experiments in hearing*. McGraw-Hill, New York.
- 362 3. Kimura, R. S. 1966. Hairs of the cochlear sensory cells and their attachment to the
 363 tectorial membrane. *Acta Otolaryngol.* 61:55-72.
- 364 4. Davis, H. 1983. An active process in cochlear mechanics. *Hear. Res.* 9:79-90.
- 365 5. Lukashkin, A. N., M. N. Walling, and I. J. Russell. 2007. Power amplification in the
 366 mammalian cochlea. *Curr. Biol.* 17:1340-1344.
- 367 6. Robles, L., and M. A. Ruggero. 2001. Mechanics of the mammalian cochlea. *Physiol.*
 368 *Rev.* 81:1305-1352.
- 369 7. Freeman, D. M., C. C. Abnet, ..., T. F. Weiss. 2003. Dynamic material properties of
 370 the tectorial membrane: a summary. *Hear. Res.* 180:1-10.
- 371 8. Gueta, R., D. Barlam, ..., I. Rousso. 2006. Measurement of the mechanical properties
 372 of isolated tectorial membrane using atomic force microscopy. *Proc. Natl. Acad. Sci.*
 373 *USA.* 103:14790-14795.
- 374 9. Richter, C.-P., G. Emadi, ..., P. Dallos. 2007. Tectorial membrane stiffness gradients.
 375 *Biophys. J.* 93:2265-2276.
- 376 10. Richardson, G. P., A. N. Lukashkin, and I. J. Russell. 2008. The tectorial membrane:
 377 one slice of a complex cochlear sandwich. *Curr. Opin. Otolaryngol. Head Neck Surg.*
 378 16:458-464.
- 379 11. Gavara, N., and R. S. Chadwick. 2009. Collagen-based mechanical anisotropy of the
 380 tectorial membrane: implications for inter-row coupling of outer hair cell bundles.
 381 *PLoS ONE.* 4:e4877.

- 382 12. Teudt, I. U., and C. P. Richter. 2014. Basilar membrane and tectorial membrane
383 stiffness in the CBA/CaJ mouse. *JARO*. DOI:10.1007/s10162-014-0463-y
- 384 13. Hubbard, A. 1993. A traveling-wave amplifier model of the cochlea. *Science*. 259:68–
385 71.
- 386 14. Russell, I. J., P. K. Legan, ..., G. P. Richardson. 2007. Sharpened cochlear tuning in a
387 mouse with a genetically modified tectorial membrane. *Nat. Neurosci.* 10:215–223.
- 388 15. Ghaffari, R., A. J. Aranyosi, and D. M. Freeman. 2007. Longitudinally propagating
389 traveling waves of the mammalian tectorial membrane. *Proc. Natl. Acad. Sci. USA*.
390 104:16510–16515.
- 391 16. Meaud, J., and K. Grosh. 2010. The effect of tectorial membrane and basilar
392 membrane longitudinal coupling in cochlear mechanics. *J. Acoust. Soc. Am.*
393 127:1411–1421.
- 394 17. Gummer, A. W., W. Hemmert, and H. P. Zenner. 1996. Resonant tectorial membrane
395 motion in the inner ear: its crucial role in frequency tuning. *Proc. Natl. Acad. Sci.*
396 *USA*. 93:8727–8732.
- 397 18. Lukashkin, A. N., G. P. Richardson, and I. J. Russell. 2010. Multiple roles for the
398 tectorial membrane in the active cochlea. *Hear. Res.* 266:26–35.
- 399 19. Jones, G. P., V. A. Lukashkina, ..., A. N. Lukashkin. 2013. Frequency-dependent
400 properties of the tectorial membrane facilitate energy transmission and amplification
401 in the cochlea. *Biophys. J.* 104:1357–1366.
- 402 20. Goodyear, R. J., and G. P. Richardson. 2002. Extracellular matrices associated with
403 the apical surfaces of sensory epithelia in the inner ear: Molecular and structural
404 diversity. *J. Neurobiol.* 53:212-227.
- 405 21. Legan, P. K., V. A. Lukashkina, ..., G. P. Richardson. 2005. A deafness mutation
406 isolates a second role for the tectorial membrane in hearing. *Nat. Neurosci.* 8:1035–
407 1042.
- 408 22. Ghaffari, R., A. J. Aranyosi, ..., D. M. Freeman. 2010. Tectorial membrane travelling
409 waves underlie abnormal hearing in *Tectb* mutant mice. *Nat. Commun.* 1:96.
- 410 23. Lukashkin, A. N., P. K. Legan, ..., G. P. Richardson. 2012. A mouse model for
411 human deafness DFNB22 reveals that hearing impairment is due to a loss of inner hair
412 cell stimulation. *Proc. Natl. Acad. Sci. USA*. 109:19351–19356.
- 413 24. Hasko, J. A., and G. P. Richardson. 1988. The ultrastructural organization and
414 properties of the mouse tectorial membrane matrix. *Hear. Res.* 35:21-38.

- 415 25. Tsuprun, V., and P. Santi. 1997. Ultrastructural organization of proteoglycans and
416 fibrillar matrix of the tectorial membrane. *Hear. Res.* 110:107–118.
- 417 26. Legan, P. K., V. A. Lukashkina, ..., G. P. Richardson. 2000. A targeted deletion in α -
418 tectorin reveals that the tectorial membrane is required for the gain and timing of
419 cochlear feedback. *Neuron.* 28:273–285.
- 420 27. Xia, A., S. S. Gao, ..., J. S. Oghalai. 2010. Deficient forward transduction and
421 enhanced reverse transduction in the alpha tectorin C1509G human hearing loss
422 mutation. *Dis. Model. Mech.* 3:209-223.
- 423 28. Simmler, M.-C., M. Cohen-Salmon, ..., J.-J. Panthier. 2000. Targeted disruption of
424 Otog results in deafness and severe imbalance. *Nat. Genet.* 24:139-143.
- 425 29. Deans, M. R., J. M. Peterson, and G. W. Wong. 2010. Mammalian Otolin: a
426 multimeric glycoprotein specific to the inner ear that interacts with otoconial matrix
427 protein Otoconin-90 and Cerebellin-1. *PLoS ONE.* 5:e12765.
- 428 30. Zheng, J., K. K. Miller, ..., P. Dallos. 2011. Carcinoembryonic antigen-related cell
429 adhesion molecule 16 interacts with α -tectorin and is mutated in autosomal dominant
430 hearing loss (DFNA4). *Proc. Natl. Acad. Sci. USA.* 108:4218-4223.
- 431 31. Freeman, D. M., K. Masaki, ..., T. F. Weiss. 2003. Static material properties of the
432 tectorial membrane: a summary. *Hear. Res.* 180:11–27.
- 433 32. Zwaenepoel, I., M. Mustapha, ..., C. Petit. 2002. Otoancorin, an inner ear protein
434 restricted to the interface between the apical surface of sensory epithelia and their
435 overlying acellular gels, is defective in autosomal recessive deafness DFNB22. *Proc.*
436 *Natl. Acad. Sci. USA.* 99:6240-6245.
- 437 33. Richardson, G. P., J. B. de Monvel, and C. Petit. 2011. How the genetics of deafness
438 illuminates auditory physiology. *Annu. Rev. Physiol.* 73:311-334.
- 439 34. Avraham, K. B., and M. Kanaan. 2012. Genomic advances for gene discovery in
440 hereditary hearing loss. *J. Basic Clin. Physiol. Pharmacol.* 23:93-97.
- 441 35. Lukashkin, A. N., M. E. Bashtanov, and I. J. Russell. 2005. A self-mixing laser-diode
442 interferometer for measuring basilar membrane vibrations without opening the
443 cochlea. *J. Neurosci. Methods.* 148:122–129.
- 444 36. Gueta, R., E. Tal, ..., I. Rousso. 2007. The 3D structure of the tectorial membrane
445 determined by second-harmonic imaging microscopy. *J. Struct. Biol.* 159:103-110.
- 446 37. Russell, I. J., M. Kossl, and G. P. Richardson. 1992. Nonlinear mechanical responses
447 of mouse cochlear hair bundles. *Proc. R. Soc. Lond. B.* 250:217-227.

- 448 38. Geleoc, G. S. G., G. W. T. Lennan, ..., C. J. Kros. 1997. A quantitative comparison of
 449 mechanoelectrical transduction in vestibular and auditory hair cells of neonatal mice.
 450 Proc. R. Soc. Lond. B. 264:611-621.
- 451 39. Masaki, K., R. Ghaffari, ..., A. J. Aranyosi. 2010. Tectorial membrane material
 452 properties in Tecta(Y)(1870C/b) heterozygous mice. *Biophys. J.* 99:3274–3281.
- 453 40. Masaki, K., T. F. Weiss, and D. M. Freeman. 2006. Poroelastic bulk properties of the
 454 tectorial membrane measured with osmotic stress. *Biophys. J.* 91:2356-2370.
- 455 41. Ghaffari, R., S. L. Page, ..., D. M. Freeman. 2013. Electrokinetic properties of the
 456 mammalian tectorial membrane. *Proc. Natl. Acad. Sci. USA.* 110:4279-4284.
- 457 42. Sellon, J. B., R. Ghaffari, ..., D. M. Freeman. 2014. Porosity controls spread of
 458 excitation in tectorial membrane traveling waves. *Biophys. J.* 106:1406-1413.
- 459 43. Weiss, T. F., and D. M. Freeman. 1997. Equilibrium behavior of an isotropic
 460 polyelectrolyte gel model of the tectorial membrane: The role of fixed charges. *Aud.*
 461 *Neurosci.* 3:351-361.
- 462 44. Farrahi, S., R. Ghaffari, and D. M. Freeman. 2011. Lowered pH alters decay but not
 463 speed of tectorial membrane waves. In WHAT FIRE IS IN MINE EARS:
 464 PROGRESS IN AUDITORY BIOMECHANICS, Proceedings of the 11th
 465 International Mechanics of Hearing Workshop. AIP Conference Proceedings 1403.
 466 403-404.
- 467 45. Freeman, D. M., S. Hattangadi, and T. F. Weiss. 1997. Osmotic responses of the
 468 isolated mouse tectorial membrane to changes in pH. *Aud. Neurosci.* 3:363-375.
- 469 46. Fisher, J. A., F. Nin, ..., A. J. Hudspeth. 2012. The spatial pattern of cochlear
 470 amplification. *Neuron.* 76:989-997.

471

472 **FIGURE LEGENDS**

473 FIGURE 1 Schematic of the inside of the experimental chamber, containing a mounted
 474 segment of TM, attached to both supports. Stimulation was delivered by the vibrating
 475 support, which was attached to a piezoelectric actuator, and a single laser was stepped along
 476 the TM to track amplitude and phase of radially shearing, longitudinally propagating
 477 travelling waves at different frequencies.

478 FIGURE 2 Phase data collected from the basal TM segments of *Tecta*^{Y1870C/+}, *Tectb*^{-/-} and
 479 *Otoa*^{EGFP/EGFP} mice. (A, B, C) Average phase lag as a function of longitudinal distance along

480 the TM segments, for each stimulus frequency (error bars are not shown for clarity). (D)
481 Average wave propagation velocity, calculated from the full longitudinal distance obtained in
482 each experiment (*Tecta*^{Y1870C/+} *n*=12, *Tectb*^{-/-} *n*=14, *Otoa*^{EGFP/EGFP} *n*=12 ±SEM), includes
483 wild-type data previously collected from the basal cochlear region for comparison (19).

484 FIGURE 3 Amplitude decay (±SD) and space constants of the travelling wave as a function
485 of frequency for basal TM segments of *Tecta*^{Y1870C/+}, *Tectb*^{-/-} and *Otoa*^{EGFP/EGFP} mice, also
486 includes previously collected wild-type data from the basal cochlear region (19). Solid lines
487 show polynomial fit to the data points.

488 FIGURE 4 Frequency dependence of the dynamic material properties of the TM. Eqs. 1 and 3
489 (Materials and Methods) and the experimental data presented in Fig. 2 C and Fig. 3 were used
490 for calculations. (A) Shear storage modulus, G' . (B) Shear viscosity, η . (C) Loss tangent,
491 $\tan(\delta)$ and (D) reciprocal of the loss tangent, $1/\tan(\delta)$, which is proportional to the quality
492 factor Q . TM thickness, T_{TM} , was taken as 20 μm for the basal segments. Includes data from
493 wild-type mice previously collected from the basal cochlear region for comparison (19).

494 FIGURE 5 Recreated instantaneous travelling waveforms calculated from the accumulated
495 phase lag and decay constant at 10 kHz and 20 kHz for all groups of mice.

496

497

498

499

500

FIGURE 1

Mounted TM

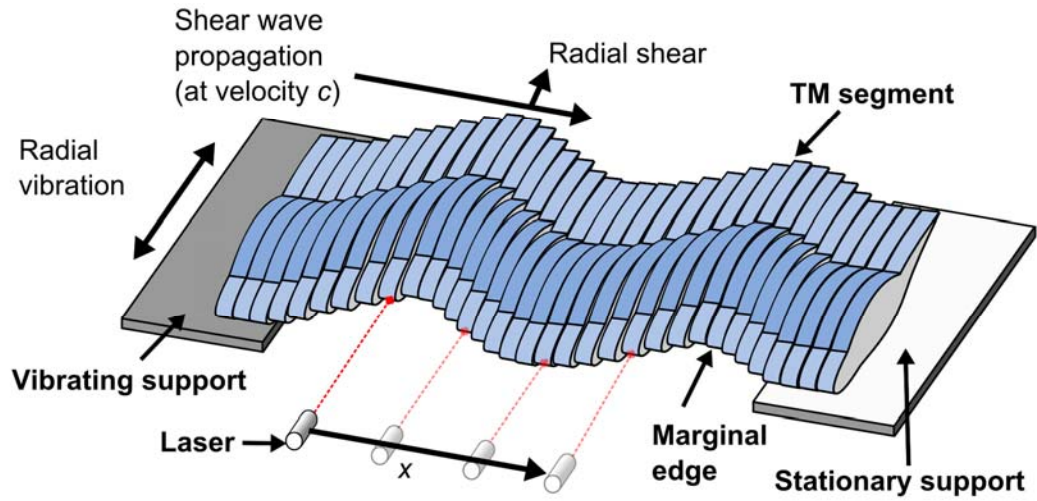


FIGURE 2

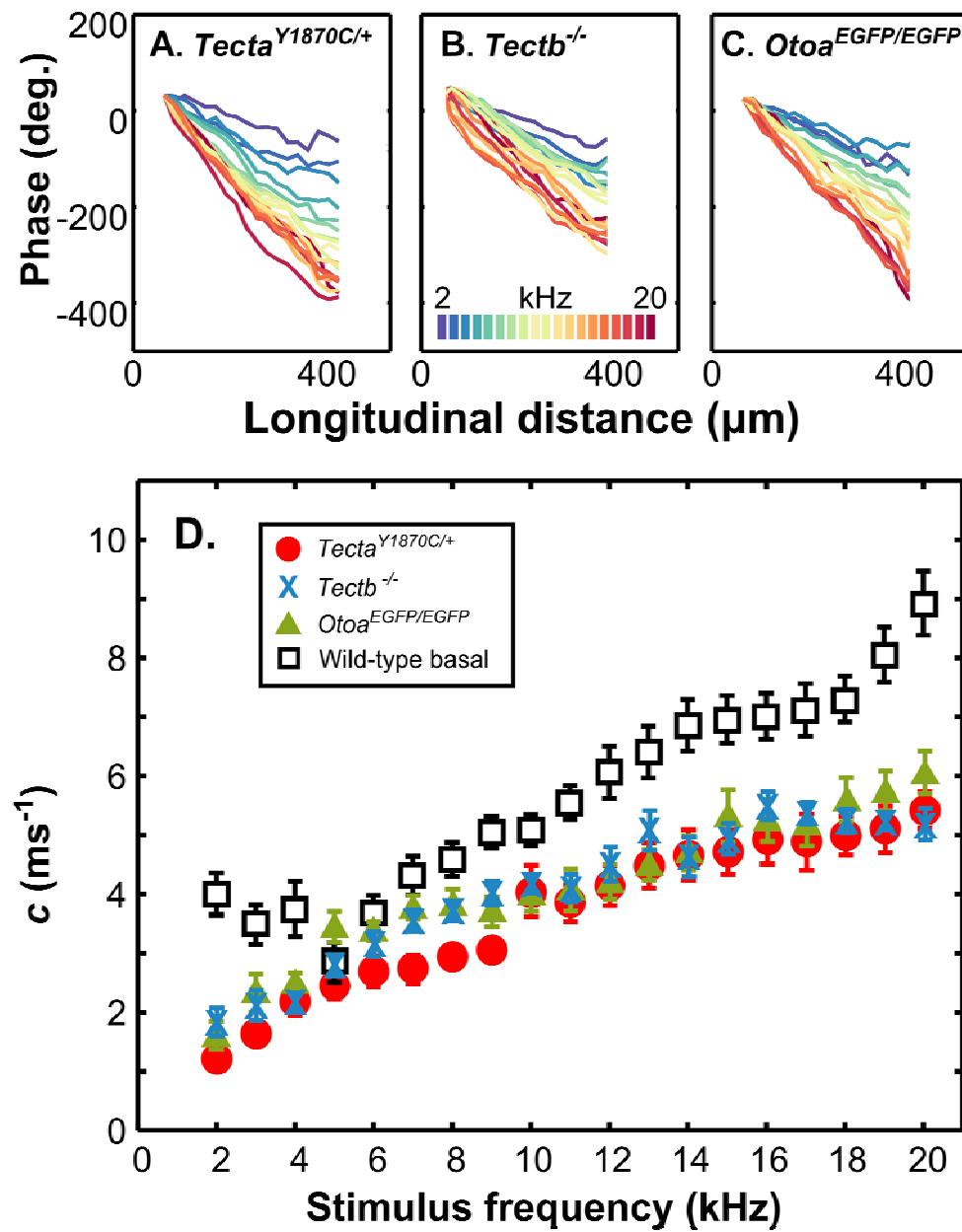


FIGURE 3

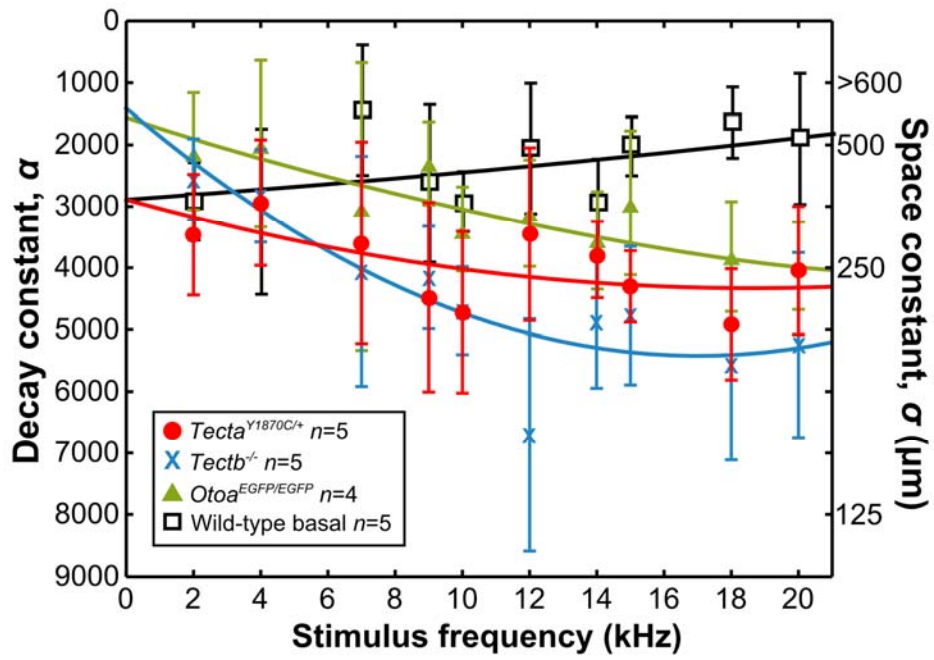


FIGURE 4

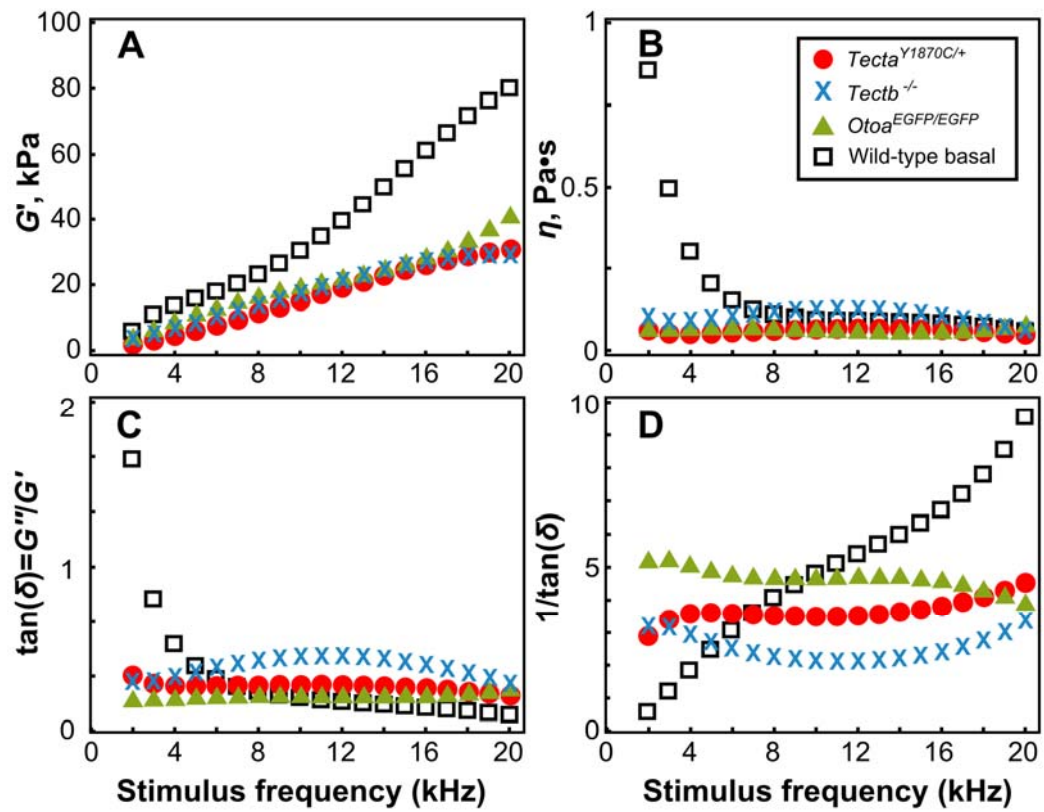


Figure 5

